Solid Freeform Fabrication 2018: Proceedings of the 29th Annual International Solid Freeform Fabrication Symposium – An Additive Manufacturing Conference
Reviewed Paper

STRUCTURALLY INTELLIGENT 3D LAYER GENERATION FOR ACTIVE-Z PRINTING

Jivtesh B. Khurana[*], Timothy W. Simpson[*†], Mary Frecker[*]
[*]Department of Mechanical and Nuclear Engineering,
[†]Department of Industrial and Manufacturing Engineering
The Pennsylvania State University, University Park, PA 16802

Abstract

Active-Z Printing offers the ability to deposit material along non-planar layers to control the mechanical behavior of parts produced by material extrusion additive manufacturing. These non-planar layers can be exploited to incorporate a part's loading conditions into the slicing process by aligning deposited layers with predicted localized stress tensors. In this work, we demonstrate that superior structural performance can be achieved by taking advantage of layer shapes derived from principal stress trajectories. A slicing method incorporating stress field data is developed to generate 3D layers from principal stress trajectories. As a demonstration, a 3-point bend specimen is manufactured with 3D layers derived from principal stress trajectories developed in a deformed specimen. Mechanical tests are conducted and 3-point bend specimens are shown to have superior mechanical response. This novel approach introduces new capabilities to Additive Manufacturing for structurally intelligent fabrication.

1. Introduction

Additive Manufacturing (AM) is the process of creating end use parts by adding material in a layer by layer manner. Material Extrusion (ME) is an AM process by which material is deposited onto a substrate by depositing layers that trace the part's cross-sectional geometry to produce 3D parts directly from CAD data[1]. These deposition platforms often consist of a gantry allowing three Degrees of Freedom (3 DoF). Consequently, the layers are restricted to 2.5D slices of the input geometry which leads to poor mechanical performance of parts due to poor bonding between layer interfaces[1, 2]. The parts produced thence have anisotropic strength and modulus that vary significantly depending on the orientation of the externally applied forces relative to the build orientation. Researchers have extensively studied these anisotropic properties and their dependence on process parameters like build temperature, feedrate, layer height, fill angle and fill density[3-13].

Researchers have developed non-planar deposition techniques for these 3 DoF systems to circumvent anisotropy arising from unidirectional planar stacking of layers. For instance, Curved Layer Fused Deposition Modeling (CL-FDM) uses non-planar layers generated through surface point data from an STL file[14]. These methods, however, are limited to geometries with surface normals that do not appreciably deviate from the vertical. CL-FDM parts shift stresses from the layer interface into the layers themselves allowing for improved mechanical performance. Singamneni et. al. used CL-FDM to improve the flexural response of a curved 3-point bend specimen by 40% when compared to a part printed using planar layers[15]. Further, the relationship between processing parameters and curved layers have been investigated. Huang et al. found that

increasing rater angle, with respect to flexural loads, negatively affects strength and adaptive layer heights are effective towards resolving sharp features in curved specimens[16].

Deposition platforms with higher DoFs offer the ability to reorient the tool head relative to the part surface opening up opportunities for effective non planar deposition strategies. Yerazunis et al demonstrated superior mechanical properties using a 5 DoF deposition system using a delta style printer and a turntable. Deposition parallel to local stress contours in a hemispherical pressure cap resulted in a 445% increase in rupture pressure as compared to planar 2-D layered pressure caps[17]. Kubalak et al. developed a 6 DoF robotic arm based extrusion platform for deposition of mechanical reinforcement skins based on composite layup patterns. Tensile specimens tested with reinforced skins oriented 45^{o} to tensile loads exhibited an 82% increase in yield strength and a 20% decrease in modulus; the decreased modulus was attributed to lower shear properties of ABS material used[18]. Furthermore, Tam et al. demonstrated a principal stress trajectory based deposition path, Stress-Line Additive Manufacturing (SLAM), that could be used as fill pattern in 3 DoF systems and as toolpath for 2.5D shells printed using a 6 DoF robotic arm. Specimens printed with SLAM showed a 100% increase in strength and up to 80% increase in elastic stiffness[19]. All the techniques mentioned above concentrate on creating layers based on a part's local surface geometry or overall shape leaving non-conventional layer shapes relatively unexplored.

Active-Z is a non-planar deposition technique developed by the authors that allows for tuning mechanical properties locally in a part by depositing layers of varying shape. Contrary to conventional AM workflow, the designer not only develops the to-be-printed part but also the layer shape corresponding to the desired mechanical properties. Using this technique, parts with sinusoidal layer shapes were demonstrated to exhibit varying strength, by up to 22.5 %, and modulus, by up to 18%, in a part by changing the amplitude, pitch and orientation of the sinusoidal layers used[20]. The focus of this paper is on incorporating a part's structural loading conditions and response to determine the ideal layer shapes to be used in Active-Z printing. In this paper, such an approach is used to improve mechanical response of a part under flexural load. A systematic workflow for incorporating a part's structural loads and limitation to deposition tool path is also presented.

The remainder of the paper is organized as follows. First, a workflow for incorporating structural loads and limitations on deposition toolpath design is presented. Next, an algorithm to derive layer shapes from principal stress trajectories is described and demonstrated for 2-D parts under various loading conditions. Then, a specific flexurally loaded geometry is used as a case study to demonstrate the proposed workflow and algorithm. Next, a physical testing plan is presented for the flexurally loaded specimens and results of mechanical tests are discussed. Finally, the benefits of incorporating the presented workflow are discussed along with the limitations of the approach and future work.

2. Active-Z Printing Workflow

Active-Z Printing is a non-planar deposition technique which uses simultaneous motion in the X, Y, and Z axes to produce additively manufactured parts. The proposed workflow to

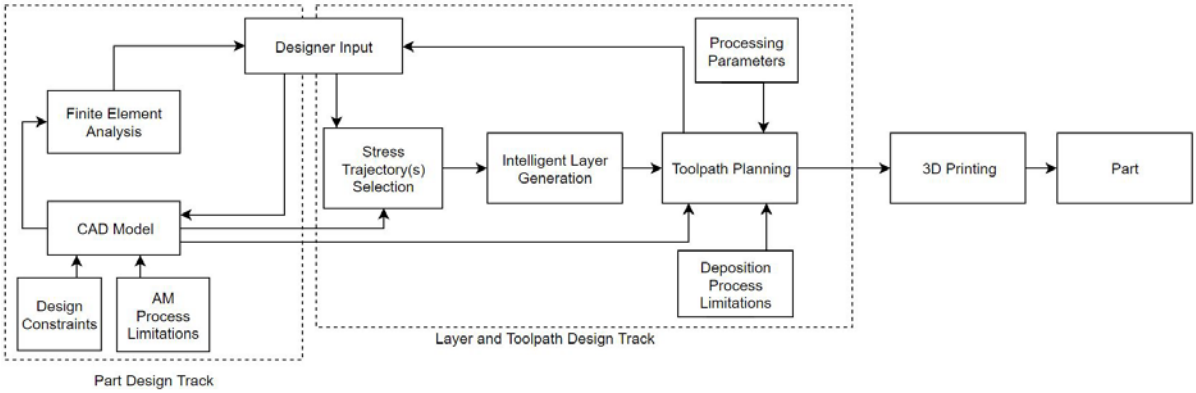

Figure 1: Active-Z Workflow for incorporation of structural loads and deposition limitations in AM build preparation.

incorporate layer design with part design and AM build preparation is shown in Figure 1. The workflow is broken down into two tracks, the first for part design and second for layer and toolpath design. The part design track consists of a CAD geometry which is improved using an appropriate finite element analysis. The Layer design track covers the design of layer shapes and deposition toolpath using AM process parameters and limitations. Next, the two feedback loops form the basis for each design track; the first loop is based on performance in a structural finite element analysis (FEA) and the second loop is based on selecting layer shapes for an appropriate mechanical response.

For the part design, a designer develops an initial CAD model based on design constraints and process limitations. Design constraints include performance and other general requirements such as size, material, stress limits, or displacement limits. AM process limitations include process-specific design constraints such as minimum wall thickness, feature size, and maximum build angle. The performance feedback loop uses results of a finite element simulation of the CAD model with appropriate material properties and boundary conditions. The results from the simulation like stress, strain, displacement and energy absorbed are used to inform the designer of the structural performance. The designer then makes changes to the initial CAD model to satisfy the initial design constraints and AM process limitations.

The layer and toolpath design track requires an understanding of correlation between layer shapes and the desired mechanical response of the part. Inputs for the layer and toolpath design track include CAD model geometry for the part and the layer shape as well as the correlation between the layer shape and its mechanical response. The toolpath generated then becomes the feedback for the designer to modify the layer to get the desired mechanical response. After incorporating the layer shape and toolpath changes, the toolpath design can be iteratively improved using the feedback loop. This optimized toolpath can then be sent to an appropriate AM machine to get the final printed part. This workflow model will be utilized for designing toolpath of a flexurally loaded part to improve its mechanical response as compared to a part built using planar layers.

3. Structurally Intelligent Toolpath Generation

The algorithm described in this section is used to generate the toolpath for the fabricating a flexurally loaded specimen with structurally intelligent layer shape design. This toolpath is

represented in Gcode language containing the location, XYZ coordinates, the feedrate and extrusion information which is readily accepted by range of AM machines across the board. The Gcode can then be executed by the AM machine using an appropriate kinematic solver.

Section 3.1 outlines the each step of the algorithm, and Section 3.2 discusses the limitations of the algorithm in its present form.

3.1 Algorithm Overview

The algorithm uses the bounding box of the part geometry and structural FEA data to generate principal stress trajectories ($PST_{(s)}$). The user then selects the desired PSTs that connect the load from the point of application to the location of structural support. An up-facing surface is also selected to define the tallest section in the part which forms the top surface. This top surface is then used to check for an end condition in the algorithm. The designer then defines a weight for each stress contour and a factor defining the rate of change in layer thickness in the specimen. A higher rate of layer thickness change allows dramatic changes in layer thickness from one layer to another. The algorithm works based on the idea of mimicking the shape of PSTs by gradually changing the shape of the deposited layers through locally increasing or decreasing the layer thickness in the part. The algorithm runs until the maximum z coordinate of the last layer is smaller than or equal to the maximum Z coordinate of the defined top surface. The generated layers are then used to create toolpath and finally Gcode for the AM machine. A graphical representation of the algorithm is presented in Figure 4 and an explanation of highlighted areas of the algorithm is detailed below, finally, examples of sliced geometries with varying layer shapes are shown in Figure 3.

3.1.1 Generation and Structural Significance of Principal Stress Trajectories

Principal Stress trajectories are integration of principal stress directions over a surface or volume. Principal stress directions can be calculated at each point in the domain by finding the Eigen vectors of the stress tensor. The vector corresponding to the largest principal stress is considered the first principal stress direction; the vector corresponding to the smallest is considered the third principal stress direction. The structural significance of PSTs is that they represent the material directions that correspond to purely axial strains devoid of shear or bending loads. The concept of PSTs are extensively used in design of large structures to determine the natural path of an applied load through a material continuum[21, 22].

PSTs are closely linked to Mitchel's theory and structural optimization[23, 24, 25]. According to Mitchel's theory, a structural material is of minimum volume if material is placed in regions where it experiences its maximum allowable tensile or compressive load given a maximum strain constraint for the structural member[26]. Given, ME systems show weaker shear and bending response due to poor inter layer and intra layer polymer welds. Aligning layers and extrusion paths parallel to principal stress trajectories based specifically on a part's loading conditions would allow for improved structural performance. PSTs are generated using an algorithm developed by Pereira et al. for plotting principal stress from discrete stress data in a 2D material domain[27]. Examples of PSTs for parts under a various loading conditions are shown in figure 2.

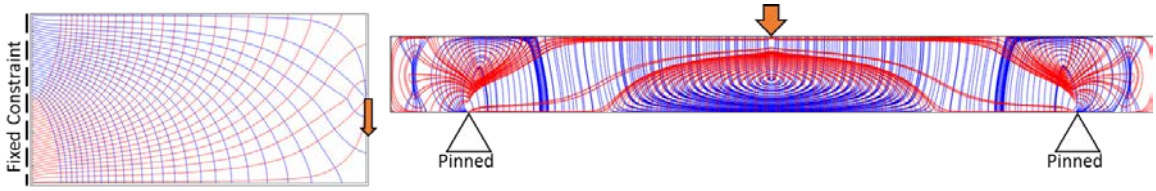

Figure 2: Principal Stress trajectories for cantilever beam and a beam under 3 point bending load. Red trajectories correspond to compressive loads while blue trajectories correspond to tensile loads.

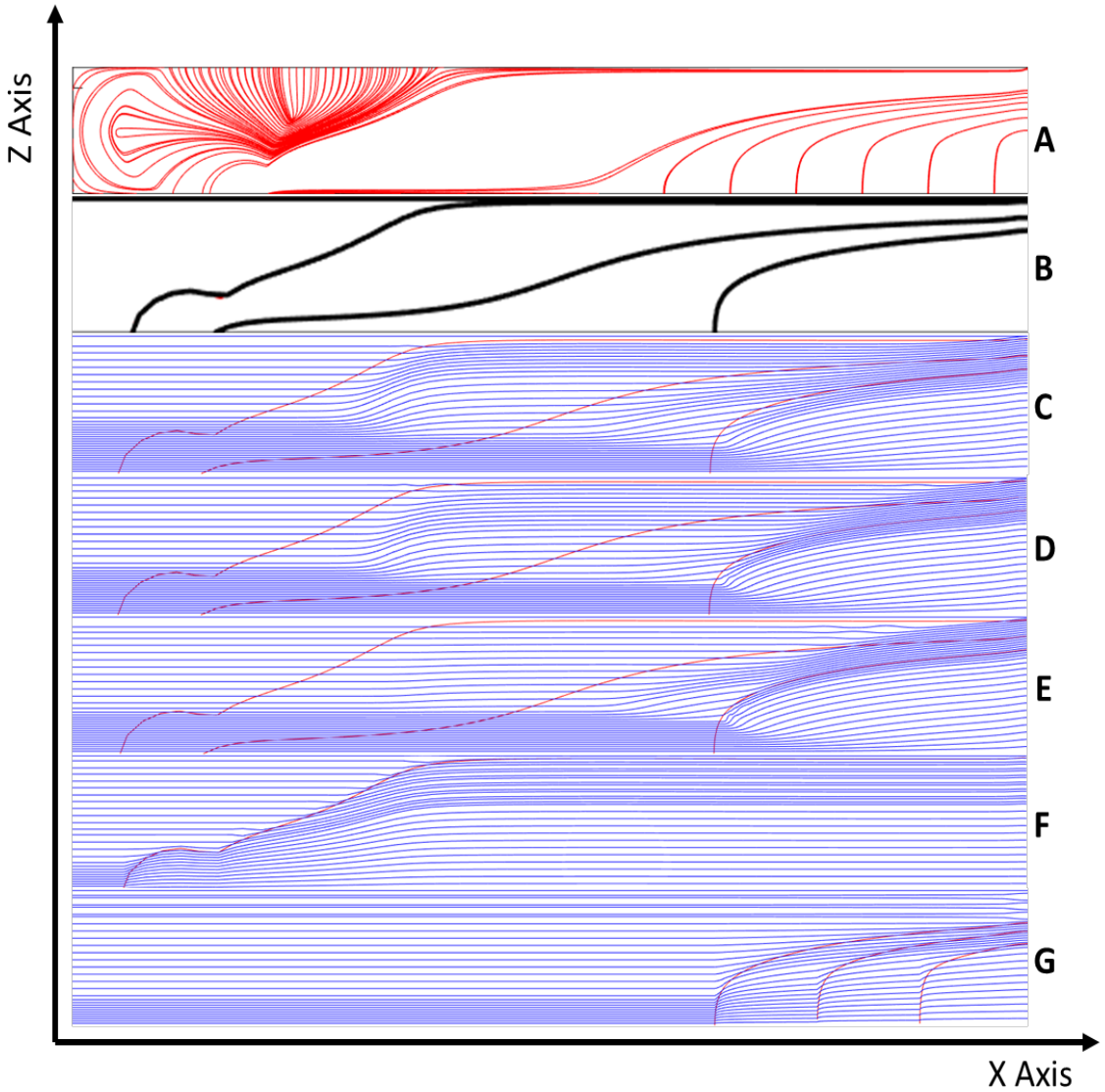

Figure 3: Principal stress trajectories for half-symmetric flexural specimen and layers sliced using them. Non-planar layers are created using locally varying layer thickness in the part. Red corresponds to PSTs, black show chosen PSTs. **A)** Shows the distribution of PCTs in a half-symmetric flexural specimen. **B)** Bold black lines represent the chosen PCTs for Layer Generation. **C to E)** Show layers generated through varying the bias weights for each principal stress trajectory. **F-G)** Layer shapes generated using different chosen stress lines.

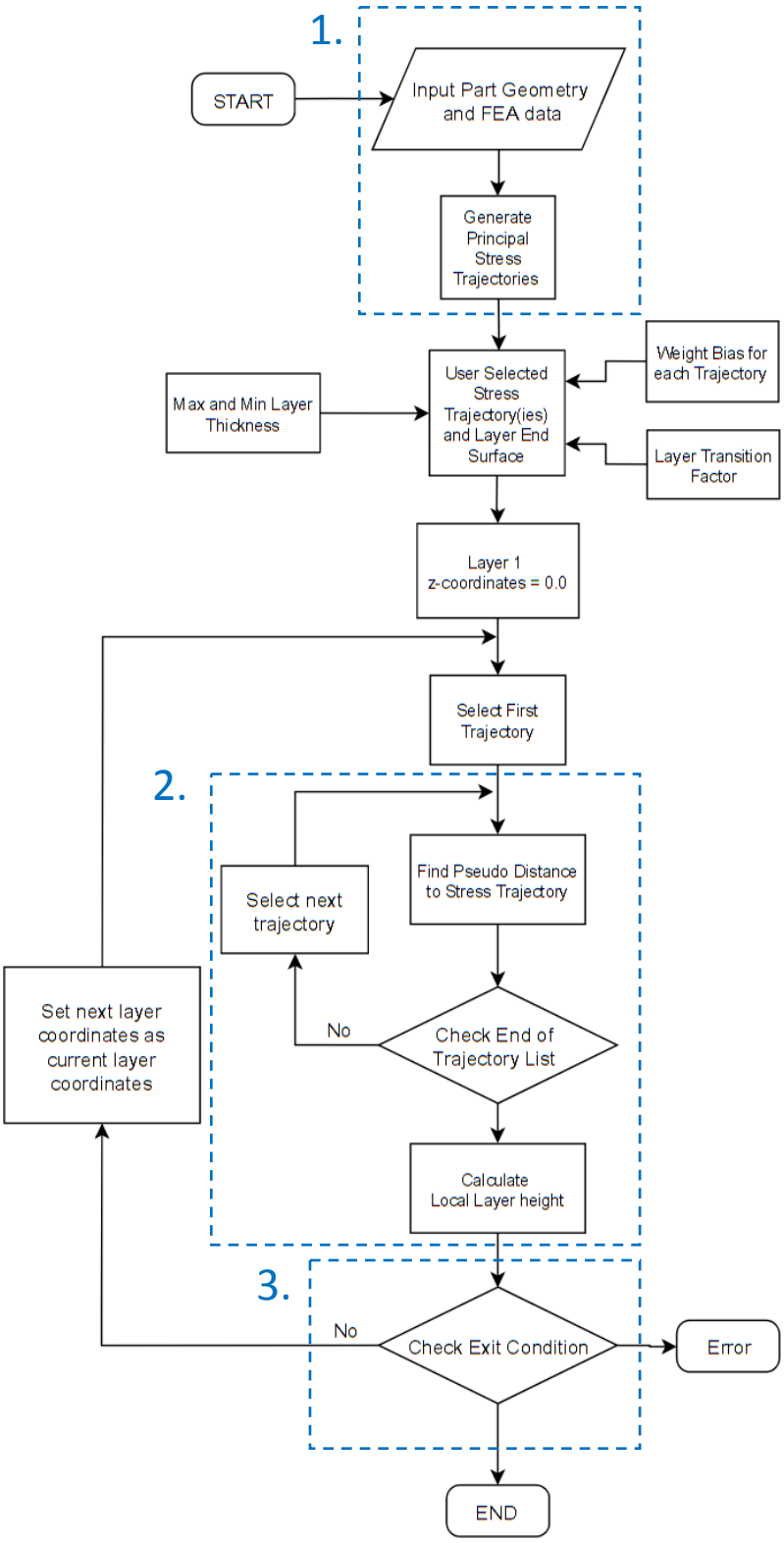

Figure 4: Graphical representation of the algorithm to generate structurally intelligent layers

3.1.2 Non Planar Layer Generation and Variable Layer Height Management

The algorithm starts by defining the initial uniform layer thickness as 0mm. A pseudo distance from the 0mm thickness layer to each chosen PST and prescribed top surface is then calculated at every point on the initial layer. The pseudo distance is calculated using equation 1 where **Π** represents the pseudo distance, $\boldsymbol{M}$ is the number of PSTs chosen by the user, $\boldsymbol{Xmax_{ps}}$ and $\boldsymbol{Xmin_{ps}}$ are the minimum and maximum $\boldsymbol{x}$ coordinate for the corresponding PST(s), $\boldsymbol{N_{ord}}$ is the rate of change in layer thickness, $\boldsymbol{W_{ps}}$ is the bias weight the for the PST $\boldsymbol{ps}$ and finally, $\boldsymbol{Z(x_j)}$ and $\boldsymbol{Z(x_{ps,j})}$ are the Z-coordinates of the current layer and PST at $\boldsymbol{x_j}$ respectively.

Equation 1:

$$\Pi = \sum_{ps=1}^{M} if\ Z(x) = \begin{cases} \dfrac{\left(Z\left(x_{ps,j}\right) - Z(x_j)\right)^{N_{ord}}}{W_{ps} \cdot Z\left(x_{ps,j}\right)}, & Z(x_j) < Z(x_{ps,j}) \\ 0, & Z(x_j) \geq Z(x_{ps,j}) \end{cases}$$
$$j \in Xmin_{ps} : Xmax_{ps}$$

The calculated pseudo distance for the layer is then normalized using the maximum pseudo distance found for the current layer. This normalized distance is then used for calculating the layer thickness for each point of the current layer using Equation 2 where $\boldsymbol{\Pi_T}$ represents the local layer thickness for every point of the current layer and; $\boldsymbol{Tmax}$ and $\boldsymbol{Tmin}$ are the maximum and minimum permissible layer thickness, respectively, based on the AM process.

Equation 2:

$$\Pi_T = \frac{\Pi \cdot (Tmax - Tmin)}{\max \Pi} + Tmin$$

The new layer is then stored and used as the starting point for calculating the thickness of the next layer. By using non-uniform thickness in a given layer non-planar layer can be formed, this progressive change in layer shape is used to mimic PSTs. This loop continues until the end condition is met.

3.1.3 Check for End Condition and Errors

Once a new layer is generated the distances to the prescribed top surface is calculated. If these distances are within the range of maximum and minimum permissible layer thickness the loop ends and the toolpath is displayed. However, if the $\max(Z_{layer}(x)) > Z_{end\ surf}$ an error is displayed. The user can correct this error by increasing the value of $\boldsymbol{N_{ord}}$ until a successful solution is found.

3.2 Algorithm Limitations

The algorithm in its present form is restricted to specific geometries and principal stress trajectory shapes, which are described below.

- The principal stress trajectory generation method used is currently only valid for 2D geometries. Consequently, the layer generation algorithm is restricted to 2.5D geometries but allows for non-uniform cross-sectional area.
- There is a minimum distance required to transition from one layer shape to another due to the limits on the layer thickness. Thus, thin geometries of the order of 3-5 times the maximum permissible layer height cannot be effectively sliced using non planar layers.
- The calculation of pseudo distance between two points is based on a one-to-one relation between sets. This means that Principal Stress Trajectories with multiple Z-coordinates for the same X-coordinate cannot be used to generate layers.
- Due to the tool-head size and normal orientation relative to the build surface, the maximum slope of each layer cannot be greater than the ratio of the nozzle's outer diameter and layer thickness at the point.
- The algorithm does not generate support material for overhanging geometries; thence overhanging sections beyond the self-supporting angle could cause poor surface finish or failure during the AM build.

4. Experimental Methods

To validate the algorithm presented in Section 3 and to determine the tensile response of a part built with non-planar structurally informed layers, three sets of flexural specimens were built and tested. In each case three PSTs, corresponding to either tensile or compressive stresses, are chosen that connect the site of the external load to the structural supports in the specimen. The chosen PSTs are given equal bias weight and a constant rate of layer thickness change of 8 is used to achieve a smooth transition between the chosen PSTs. A maximum layer thickness of 0.3mm and a minimum layer thickness of 0.1mm was prescribed. The extrusion rate for the process was kept constant while the federate of the end effector was changed to vary material deposition rate during the build. Figure 5 shows a comparison between the computed layer pattern and an as printed geometry.

The specimens are designed according to the ASTM D790 standard for measuring flexural properties of plastics. The specimens are 100mm long, 12.5mm wide and 6mm thick. A support span of 80mm and an overhang length of 10mm is used. The specimens were printed in the standard XYZ orientation on a SeeMeCNC Rostock Max V2 with Poly Lactic Acid (PLA) filament. The parts were manufactured to be fully dense and the fill pattern, in the X-Y plane, alternates between 45^{o} and 135^{o} from the X axis every other layer. Parts were printed at a uniform speed of 1800mm/min with an extrusion temperature of 210 ± 2^{o} C and a print surface temperature of 65 ± 1 ^{o} C, as recommended by the filament manufacturer. All temperature measurements were taken using a 100K EPCOS thermistors rated for temperature measurement up to 300^{o} C. Each specimen was printed individually, a total of 15 build trays were printed in this study. Following the completed print job, the build plate was allowed to cool down from 65 ± 2^{o} C to 35 ± 2^{o} C before the specimens were removed to minimize warping. Upon removal,

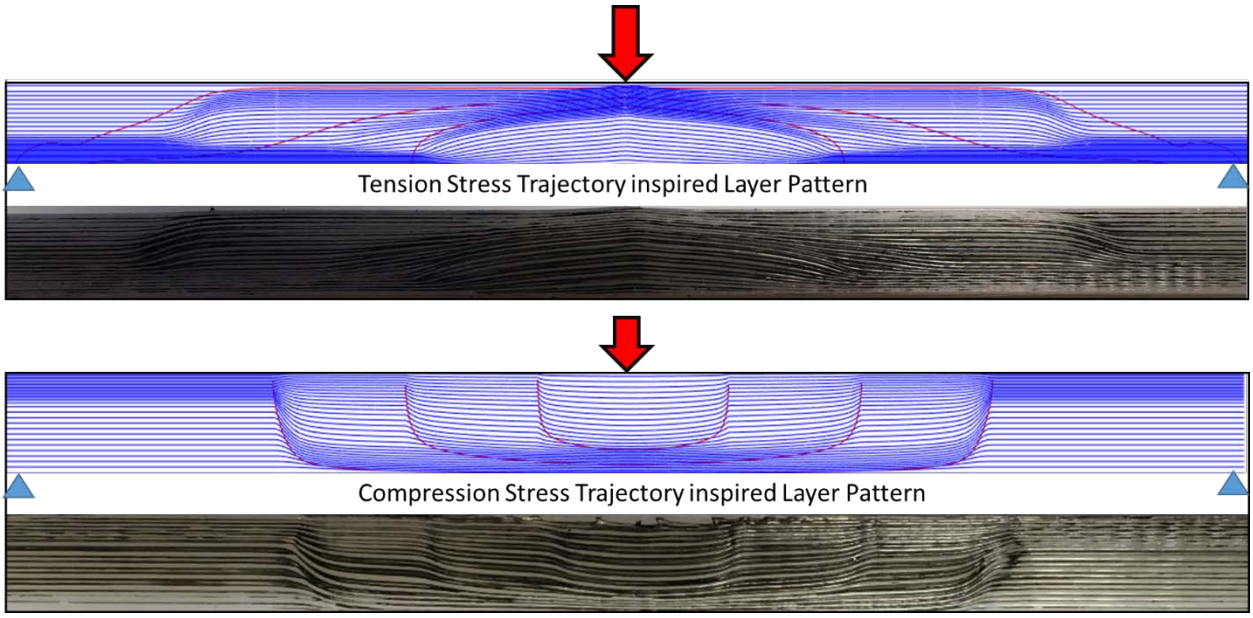

Figure 5: Layer Pattern generated by principal stress trajectories corresponding to printed specimens

the specimens were stored in an airtight transparent bag in a metal cabinet located away from potential sources of moisture.

Flexural Tests were conducted using a Shimadzu Autograph AGSX machine with a 1KN load cell. Specimen deflection was measured using crosshead position in accordance to the D790 standard testing procedure. Five specimens of each type were tested and a mean for each measured mechanical property is calculated. A photo of the delta configuration extrusion platform used is shown in figure 6a, a schematic of the specimen geometry is shown in figure 6b, and the testing setup is pictured in Figure 6c.

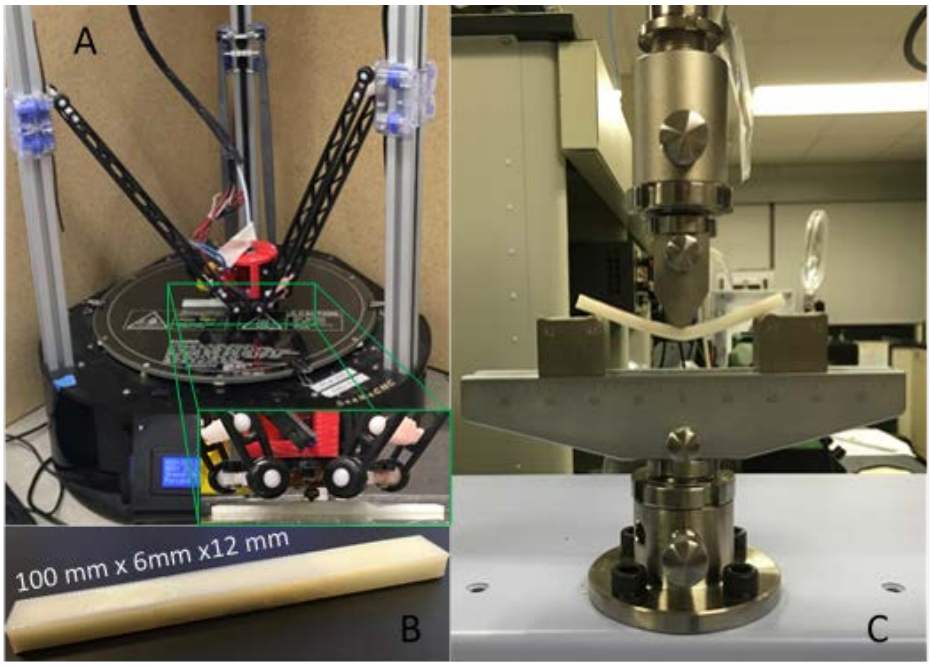

Figure 6: A) Delta printer used to manufacture test specimens, B) Active-Z Specimen with non-planar layers, C) Mechanical setup used to conduct flexural testing

5. Results and Discussions

A comparison of the flexural modulus and strength for the three printed specimens are shown in figure 7. The specimens printed with tensile PSTs were found to have a 12.25% increase in strength and a 22.75% increase in modulus while the specimens printed using compressive PSTs demonstrated an increase of 7.13% in strength and 16.38% in modulus. Given the fill patterns were oriented 45° to the direction of the tensile load experienced in the bending specimen, a combination shear and tensile failure was expected for the test specimens. The fracture surfaces showed a saw tooth failure pattern similar to Ziemian et al.[5] Further, specimens corresponding to tensile PSTs were V-shaped as compared to transverse failure with local saw tooth patterns found in the compressive PST specimen, see figure 8.

Figure 8: Fracture surfaces showed local saw-tooth pattern similar to Ziemian et al.

The increases in the stiffness and modulus can be attributed to two factors. First, the use of layers mimicking PSTs allow for filaments to experience a larger individual force allowing for a gain in the strength. The other contribution to the increase in strength and modulus is the distribution of more number of thinner layers across the tensile region in the flexural specimen. Thinner layers are known to have higher tensile strength and modulus[6]. The compressive PSTs comprised of thinner layers in the tensile region and thicker layers in the compressive zone can be seen in figure 6.

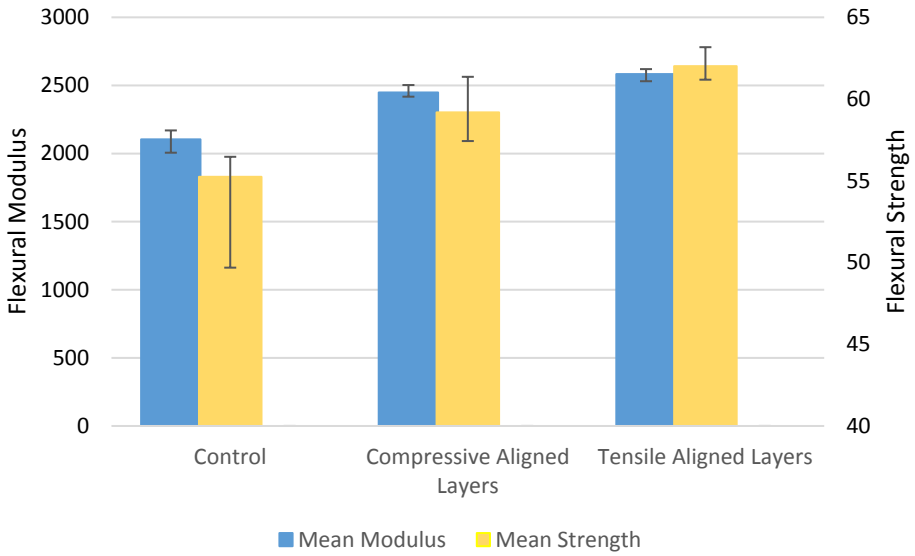

Figure 7: Higher flexural modulus and flexural strength was overserved for principal stress aligned layers

6. Closure

This paper introduced an AM workflow for incorporating structural loads and limitations on deposition paths for structurally intelligent toolpaths. Further, an algorithm used to derive non planar layers from structural finite element data is presented. Finally, mechanical tests are conducted to compare principal stress trajectory inspired layer pattern with conventional 2.5D layer pattern. The control specimens had a mean flexural strength of 55.24 MPa and flexural modulus of 2.104 GPa. The compressive principal stress aligned flexural specimens demonstrated a mean strength of 59.18 MPa and a modulus of 2.448 GPa, an increase of 7.13% and 16.38%. The tensile principal stress aligned flexural specimens had a mean flexural strength of 62.013 MPa and a modulus of 2.583 GPa, an increase of 12.25% and 22.75% respectively. The increase in strength is attributed to individual filaments experiencing larger force and the distribution of thinner layers known to exhibit higher strength and modulus. The fracture show a combination of tensile and shear failure evident from the saw tooth pattern of the fracture surface.

Principal stress trajectories chosen for this paper are based on the author's understanding of the workflow and slicing algorithm. Further analysis is required to understand how selection of certain principal stress trajectories impacts the mechanical behavior. Also, a quantitative method for PST selection needs to be incorporated in the Active-Z algorithm itself. Another area for improvement for principal stress aligned layers would be for materials that exhibit high amount of material anisotropy. For instance, the strength ratio between X-axis and Z axis specimens for 13% carbon fiber filled ABS is 2.94[28]. Thus, a material like CF-ABS would benefit much more by aligning the layers and deposition paths along the applied load.

The algorithm presented is currently limited to 2.5D geometries, however, the methodology of aligning layers and deposition paths to the principal stress trajectories can easily

be expanded to more complex 3D geometries. Further, mechanical parts can experience complex loading conditions when under use, the authors look forward to expanding the current technique to include more complex loading conditions and composite materials properties.

7. Acknowledgements

The authors would like to thank Dr. Paris VonLockette at Penn State University for access to universal testing equipment in his lab. We also acknowledge Nathan Watson at Penn State for his assistance in mechanical testing.

References

1. Gibson, I., Rosen, D. W. & Stucker, B. *Additive Manufacturing Technologies: Rapid Prototyping to Direct Digital Manufacturing*, Springer, New York, 2010.
2. Ahn, Sung-Hoon, Montero, M., Odell, D., Roundy, S., & Wright, P. K "Anisotropic Material Properties of Fused Deposition Modeling ABS." *Rapid Prototyping Journal*, vol. 8, no. 4, Oct. 2002, pp. 248–257.
3. Mohamed, Omar A., Syed H. Masood, and Jahar L. Bhowmik. "Optimization of Fused Deposition Modeling Process Parameters: A Review of Current Research and Future Prospects." *Advances in Manufacturing* 3.1 (2015): 42-53.
4. Said Es, J. Os Foyos, R. Noorani, M. Mandelson, R. Marloth, B.A. Pregger "Effect of layer orientation on mechanical properties of rapid prototyped samples" *Materials and Manufacturing Process* 15 (1) (2000): pp. 107–122.
5. Ziemian, Constance, Mala Sharma, and Sophia Ziemian. "Anisotropic mechanical properties of ABS parts fabricated by fused deposition modelling". INTECH Open Access Publisher, 2012
6. Sood, Anoop Kumar, R.k. Ohdar, and S.s. Mahapatra. "Parametric Appraisal of Mechanical Property of Fused Deposition Modelling Processed Parts." *Materials & Design*, Vol. 31 Issue: 1, pp.287-95, 2010
7. A.K. Sood, R.K. Ohdar, and S.S. Mahapatra. "Experimental Investigation and Empirical Modelling of FDM Process for Compressive Strength Improvement." *Journal of Advanced Materials*, Vol. 3 Issue: 1, pp.81-90, 2011
8. J. Laeng, Zahid A. Khan and S.Y. Khu, 2006. "Optimizing Flexible Behaviour of Bow Prototype using Taguchi Approach." *Journal of Applied Sciences*, Vol. 6 Issue: 3, pp.622-630, 2006
9. Wang, Ming Tian, Tong Xi Jun, Ye Jin "A Model Research for Prototype Warp Deformation in the FDM Process" *International Journal of Advanced Manufacturing Technology*, Vol 33 Issue 11–12, pp.1087–1096, 2007
10. C.T. Bellehumeur, L. Li, Q. Sun, P. Gu. "Modeling of Bond Formation between Polymer Filaments in the Fused Deposition Modeling Process" *Journal of Manufacturing Processes,* Vol. 6 Issue: 2, pp.170-178, 2004

11. C.T. Bellehumeur, P. Gu, Q. Sun, G.M. Rizvi. “Effect of Processing Conditions on the Bonding Quality of FDM Polymer Filaments” *Rapid Prototyping Journal*, Vol. 14 Issue: 2, pp. 72–80, 2008
12. Bartolai, Joseph, Timothy W. Simpson, and Renxuan Xie. "Predicting Strength of Thermoplastic Polymer Parts Produced using Additive Manufacturing." *Solid Freeform Fabrication Symposium*, Austin, TX. 2016.
13. Page, James Sherwood. “Systems and Methods for Improving 3D Printing”. Autodesk, Inc, assignee. Patent US 14/663,393. 24 Sept. 2015. Print
14. D. Chakraborty, B. A. Reddy, and R. Choudhury, "Extruder Path Generation for Curved Layer Fused Deposition Modeling," *Computer Aided Design*, Vol. 40, pp. 235-243, 2008
15. Singamneni, Sarat, Asimava Roychoudhury, Olaf Diegel, and Bin Huang. "Modeling and Evaluation of Curved Layer Fused Deposition." *Journal of Materials Processing Technology* 212.1 (2012): 27-35.
16. B. Huang, S. Singamneni, "Curved Layer Adaptive Slicing (CLAS) for fused deposition modelling", *Rapid Prototyping Journal*, Vol. 21 Issue: 4, pp. 354-367, 2015
17. Yerazunis, William S. "Strengthening ABS, Nylon, and Polyester 3D Printed Parts by Stress Tensor Aligned Deposition Paths and Five-Axis Printing." Proceedings of the Solid Freeform Fabrication Symposium, AT&T Conference Center, Austin, Texas. 10 Aug. 2016. Web. 15 Nov. 2016.
18. Joseph R. Kubalak, Alfred L. Wicks & Christopher B. Williams (2017) Using multi-axis material extrusion to improve mechanical properties through surface reinforcement, Virtual and Physical Prototyping, 13:1, 32-38
19. Tam, Kam-Ming Mark and Caitlin T. Mueller. “Additive Manufacturing Along Principal Stress Lines.” 3D Printing and Additive Manufacturing, 4:2, pp. 63–81, 2017
20. Khurana, Jivtesh B., Shantanab Dinda and Timothy W.. Simpson. "Active-Z Printing: A New Approach to Increasing 3D Printed Part Strength." Proceedings of the Solid Freeform Fabrication Symposium, Austin, TX. 2017
21. Fonseca J. The loadpath-a way to understand the quality of structures. J (IASS) 1997;38:129–135. 29.
22. Michalatos P, Kaijima S. Eigenshells: Structural patterns on modal forms. In: Shell Structures for Architecture: Form Finding and Optimization. Routledge, New York City, NY, 2014; pp.195–210
23. Chen Y, Li Y. Beam Structure Optimization for additive manufacturing based on principal stress lines. Proceedings of the 21st Solid Freeform Fabrication (SFF) Symposium. Austin, TX: SFF, 2011; pp.666–678.
24. Hemp WS. Optimum Structures. Oxford: Oxford University Press, 1973, p.71.
25. Strang G, Kohn R. Hencky-Prandtl nets and constrained Michell trusses. Computational Methods & Applied Mechanical Engineering, 36, pp. 207–222, 1983
26. A. S. L. Chan (1962) The Design of Michell Optimum Structures, Aeronautical Research Council Reports and Memoranda, Ministry of Aviation, London England.
27. O.J.B.Almeida Pereira, J.P.B.Moitinho de Almeida, Automatic drawing of stress trajectories in plane systems, Computers & Structures, Volume 53, Issue 2, 1994, Pages 473-476, ISSN 0045-7949

28. C. E. Duty, V. Kunc, B. Compton, B. Post, D. Erdman, R. Smith, R. Lind, P. Lloyd, and L. Love, Structure and mechanical behavior of big area additive manufacturing (baam) materials," Rapid Prototyping Journal, vol. 23, no. 1, pp. 181-189, 2017.